



INEEL/CON-04-01694
PREPRINT

Seismic Transducer Modeling Using ABAQUS

S. R. Novascone
M. J. Anderson
K. D'Souza

May 25-27, 2004

ABAQUS Users Conference

This is a preprint of a paper intended for publication in a journal or proceedings. Since changes may be made before publication, this preprint should not be cited or reproduced without permission of the author.

This document was prepared as an account of work sponsored by an agency of the United States Government. Neither the United States Government nor any agency thereof, or any of their employees, makes any warranty, expressed or implied, or assumes any legal liability or responsibility for any third party's use, or the results of such use, of any information, apparatus, product or process disclosed in this report, or represents that its use by such third party would not infringe privately owned rights. The views expressed in this paper are not necessarily those of the U.S. Government or the sponsoring agency.

Seismic transducer modeling using ABAQUS

S. R. Novascone¹, M. J. Anderson², and K. D'Souza³

¹Idaho National Engineering and Environmental Laboratory

²University of Idaho

³ABAQUS

Abstract: A seismic transducer, known as an orbital vibrator, consists of a rotating imbalance driven by an electric motor. When suspended in a liquid-filled wellbore, vibrations of the device are coupled to the surrounding geologic media. In this mode, an orbital vibrator can be used as an efficient rotating dipole source for seismic imaging. Alternately, the motion of an orbital vibrator is affected by the physical properties of the surrounding media. From this point of view, an orbital vibrator can be used as a stand-alone sensor. The reaction to the surroundings can be sensed and recorded by geophones inside the orbital vibrator. These reactions are a function of the media's physical properties such as modulus, damping, and density, thereby identifying the rock type. This presentation shows how the orbital vibrator and surroundings were modeled with an ABAQUS acoustic FEM. The FEM is found to compare favorably with theoretical predictions. A 2D FEM and analytical model are compared to an experimental data set. Each model compares favorably with the data set.

Keywords: Seismic, Acoustics, and Wellbore.

1. Introduction

Seismic waves have been used for many decades to investigate the geometric and spatial extent of various geological media. More recently, they are being used to extract intrinsic mechanical properties of the geologic media and the fluids that fill them. Consequently, property investigations of the geologic subsurface is important to the energy industry for the purpose of locating and extracting fossil fuels (Chang and others, 1998) and to the environmental industry for understanding subsurface contaminate fate and transport (National Research Council, 2000). Examples of investigating geological properties using seismic waves are the use of continuous frequency acoustic transducer borehole loggers to measure the wave speed of geologic media surrounding a well (Brie and others 1998) and the application of reflection tomography to locate boundaries in a heterogeneous media (Paillet and Cheng, 1991). In principle, an alternate way to measure or infer properties of geologic media using seismic waves is to measure the vibration of an acoustic/seismic transducer with a motion sensor that is attached to the transducer. Because the

transducer is mechanically coupled to the surrounding geologic medium, its motion may be influenced by properties such as elastic modulus, density, and wave speed of the geologic medium. Thus in principle, the motion of the transducer could be used to infer the elastic properties of the geological medium or to detect a change in elastic properties as a function of borehole depth. In this paper, a measurement of this type is referred to as driving-point impedance.

One such seismic transducer is an orbital vibrator. It has been used as a source of seismic waves in cross-well seismic surveys (Daley and Cox, 2001). An orbital vibrator is a rotating eccentric mass contained within a closed cylinder. The rotation of the eccentric mass is powered by an electric motor. The orbital vibrator is suspended vertically by a seven-conductor wire line, through which power and motion sensor signals are transferred. A sketch of an orbital vibrator is shown in Figure 1, which includes the motor, rotating eccentric mass, cylinder, wire line and axes of the oscillation plane. The rotating eccentric mass exerts a force on the cylinder, which in turn couples through the fluid in the well to the surrounding geologic medium, thus causing a rotating dipole in the geologic medium. When suspended vertically in a vacuum, the orbital vibrator translates in a circular orbit in the horizontal x - y plane defined by the axes in Figure 1, but does not rotate. Figure 2 shows a side view of an orbital vibrator located in a liquid-filled well surrounded by an elastic medium.

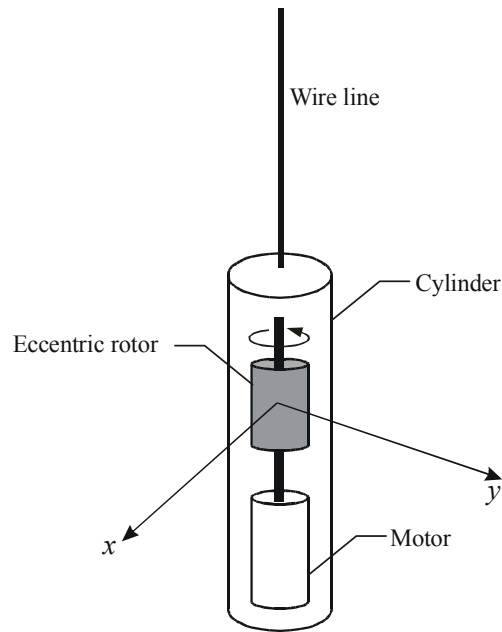


Figure 1. Orbital vibrator seismic source.

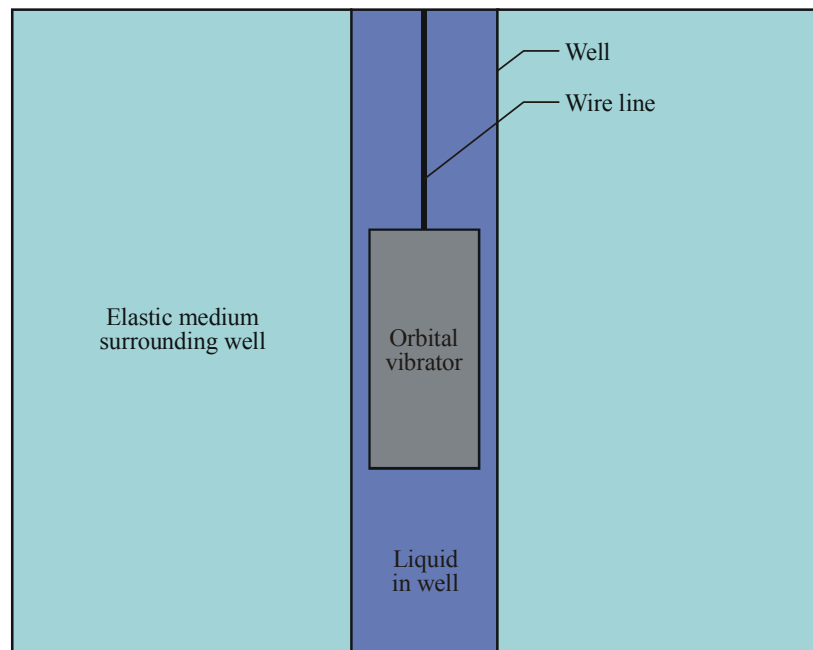


Figure 2. Orbital vibrator in liquid-filled well.

To use the driving-point impedance feature of the orbital vibrator in practice, one must quantitatively demonstrate that the motion of an orbital vibration source is sensitive to the properties of geologic media. Additionally a mathematical model must be available for determining which geologic media properties cause a measurable effect on the motion of an orbital vibrator. Some of the work performed thus far to attain such a model is presented in this paper. It is shown here how the orbital vibrator and surroundings were modeled with an ABAQUS acoustic FEM. The FEM is found to compare favorably with theoretical predictions. A 2D FEM and analytical model are compared to an experimental data set. Each model compares favorably with the data set.

2. Modeling

The analytical model that is discussed in this paper was presented by Reynolds and Cole (2002), which is a solution to the wave equation in terms of pressure in the water and displacement in the elastic medium in 2D. The Reynolds and Cole model treats the orbital vibrator as a cylinder coupled to an elastic medium by a liquid in an annulus between the cylinder and elastic medium. An applied harmonic force whose magnitude is assumed to be proportional to the square of the frequency causes the motion of the cylinder.

The orbital vibrator seismic source was modeled as a cylinder of radius a surrounded by a liquid-filled annulus of radius b . The annulus is bounded by an elastic isotropic medium of infinite

extent. The cylinder was assumed to be rigid with mass per unit length M . Motion of the cylinder due to the applied harmonic force was in the x -direction and of the form $me\omega^2\sin\omega t$ (rotating mass imbalance, Steidel, 1989), where m is the eccentric mass per unit length, e is the dimension of the eccentricity, and ω is the circular frequency. An illustration of this model is shown in Figure 3.

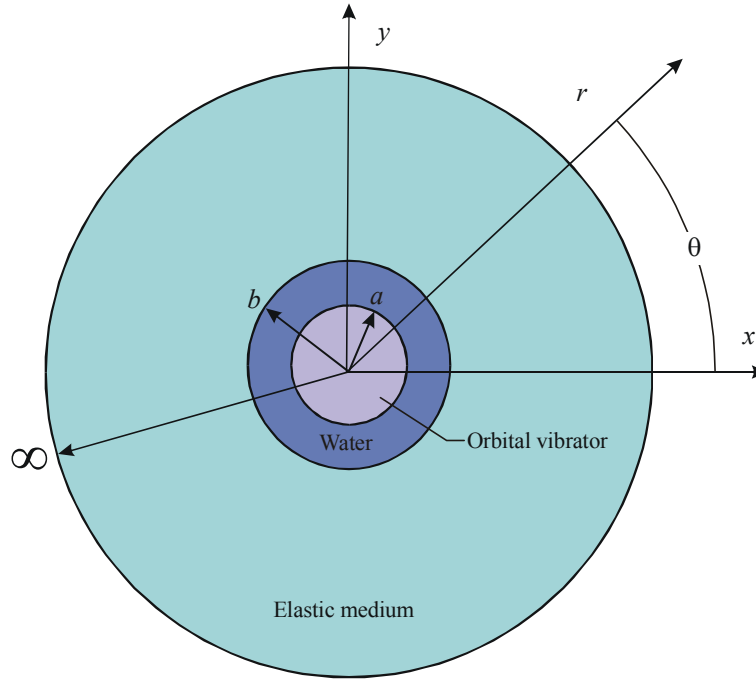


Figure 3. Two-dimensional orbital vibrator in water-filled well surrounded by unbounded elastic medium.

The motion of the cylinder was determined by the acceleration of the eccentric mass and the acoustic pressure in the surrounding liquid. The effect of the rotating eccentric mass is periodic forces acting on the cylinder in the x - y plane. These periodic forces will cause the cylinder assembly to translate in a circular orbit in the x - y plane. This motion can be represented as a superposition of harmonic motion in the x - and y -directions with a one-quarter period phase lag. It is therefore adequate to use the solution for harmonic motion of the vibrator along one axis to characterize its behavior. The axis used for this calculation was the x -axis. A cylindrical coordinate system was used for the analysis where r is the distance from the origin and θ is the angle, measured positive counter-clockwise from the x -axis. The acoustic pressure $p(r, \theta)e^{j\omega t}$ in the liquid was

$$p(r, \theta) = [AH_1^{(1)}(k_p r) + BH_1^{(2)}(k_p r)]\cos(\theta) \quad (1)$$

(Williams, 1999) where A and B are arbitrary coefficients, $k_p = \omega/c_p$ is the wave number in water, c_p is the sound velocity in water, and $H_1^{(1)}$ and $H_1^{(2)}$ are Hankel functions of order 1. $H_1^{(1)}$

represents the reflected or incoming wave and $H_1^{(2)}$ represents the propagating or outgoing wave.

In the elastic solid, the displacement $\bar{u}(r, \theta) e^{j\omega t}$ was

$$\bar{u} e^{j\omega t} = [u_r(r, \theta) \hat{e}_r + u_\theta(r, \theta) \hat{e}_\theta] e^{j\omega t} = \{\nabla \phi + \nabla \times [\psi(r, \theta) \hat{e}_z]\} e^{j\omega t} \quad (2)$$

where u_r and u_θ are the displacement components in the radial and circumferential directions, $\phi(r, \theta)$ and $\psi(r, \theta) \hat{e}_z$ are the scalar and vector displacement potentials for longitudinal and shear displacements, and \hat{e}_r , \hat{e}_θ , and \hat{e}_z are the unit vectors in the radial, tangential, and axial directions respectively. The displacement potentials $\phi(r, \theta)$ and $\psi(r, \theta)$ in the elastic solid were

$$\phi(r, \theta) = CH_1^{(2)}(k_L r) \cos(\theta), \quad \psi(r, \theta) = DH_1^{(2)}(k_S r) \sin(\theta), \quad (3, 4)$$

where C and D are arbitrary coefficients, $k_L = \omega/c_L$ and $k_S = \omega/c_S$ are the longitudinal and shear wave numbers; c_L and c_S are the longitudinal and shear wave speeds in the elastic solid. Note that for the solid only the outgoing waves are included in the model such that an infinite medium is modeled.

The coefficients A , B , C , and D were determined by boundary conditions. At $r = a$, the equation of motion for the rigid cylinder gave

$$\left. \frac{\partial p}{\partial r} \right|_{r=a} = \frac{-\rho \cos \theta}{M} [m e \omega^2 - \int_0^{2\pi} p(a, \theta) a \cos \theta d\theta] \quad (5)$$

where ρ is the mass density of the liquid. The remaining boundary conditions are obtained through the application of continuity in displacements and normal stress, and the vanishing of shear stress at $r = b$

$$\left. \frac{\partial p}{\partial r} \right|_{r=b} = -\rho \frac{\partial^2 u_r}{\partial t^2}, \quad (-p = \sigma_r)|_{r=b}, \quad \tau_{r\theta}|_{r=b} = 0. \quad (6, 7, 8)$$

In the above expressions, σ_r and $\tau_{r\theta}$ are the radial and tangential stresses in the elastic solid, where since this was a two-dimensional model the plane-strain assumption for the constitutive relationship is used (Malvern, 1969). The boundary conditions (6) – (8) are typical for fluid-structure interaction problems (Ihlenburg, 1998). Adherence to the boundary conditions (5) – (8) requires that the coefficients A , B , C and D satisfy

$$[G] \begin{Bmatrix} A \\ B \\ C \\ D \end{Bmatrix} = \begin{Bmatrix} -\rho m e \omega^2 \\ M \\ 0 \\ 0 \\ 0 \end{Bmatrix} \quad (9)$$

where the non-zero elements of $[G]$ are given by the following equations.

$$G_{11} = H_1^{(1)'}(k_p a) - \frac{a\pi\rho}{m_{OV}} H_1^{(1)}(k_p a), \quad G_{12} = H_1^{(2)'}(k_p a) - \frac{a\pi\rho}{m_{OV}} H_1^{(2)}(k_p a),$$

$$G_{21} = H_1^{(1)'}(k_p b), G_{22} = H_1^{(2)'}(k_p b), G_{23} = -\rho\omega^2 H_1^{(2)'}(k_L b), G_{24} = -\frac{\rho\omega^2}{b} H_1^{(2)}(k_S b),$$

$$G_{31} = -H_1^{(1)}(k_p b), G_{32} = -H_1^{(2)}(k_p b),$$

$$G_{33} = -\left[(\lambda + 2\mu) H_1^{(2)''}(k_L b) - \frac{\lambda}{b^2} H_1^{(2)}(k_L b) + \frac{\lambda}{b} H_1^{(2)'}(k_L b) \right],$$

$$G_{34} = -2\mu \left(-\frac{1}{b^2} H_1^{(2)}(k_S b) + \frac{1}{b} H_1^{(2)'}(k_S b) \right), G_{43} = -\frac{2}{b} H_1^{(2)'}(k_L b) + \frac{1}{b^2} H_1^{(2)}(k_L b),$$

and

$$G_{34} = -2\mu \left(-\frac{1}{b^2} H_1^{(2)}(k_S b) + \frac{1}{b} H_1^{(2)'}(k_S b) \right).$$

Note that the prime (') indicates the derivative taken with respect to the argument of the Hankel function. In the above expressions for the elements of $[G]$, λ and μ are the Lamé coefficients for the elastic solid. The rows of $[G]$ correspond respectively to the boundary conditions (5)-(8).

The analytical model was compared to an ABAQUS finite element model. Figure 4 shows a picture of the finite element model that is scaled so that the main features of the model are discernable on a single picture. Figure 4 shows the green orbital vibrator elements, the magenta interface elements, the blue acoustic elements, the dark green elastic medium elements, and the cyan infinite elements. Also shown in Figure 4 is the location and direction of the oscillating point load. For the elastic continuum, ABAQUS CPE4 finite elements were used. The CPE4 element is a plain-strain, four-node, linear, continuum element. The active degrees of freedom at each node for the CPE4 are the displacements in the x - and y -directions (see Figure 4). The water in the annulus between the orbital vibrator and the elastic medium was modeled with ABAQUS AC2D4 elements. The AC2D4 is an acoustic, four-node, linear, continuum element. The active degree of freedom at each node for the AC2D4 element is the acoustic pressure. The analysis type was steady state dynamics direct where frequency and load were specified.

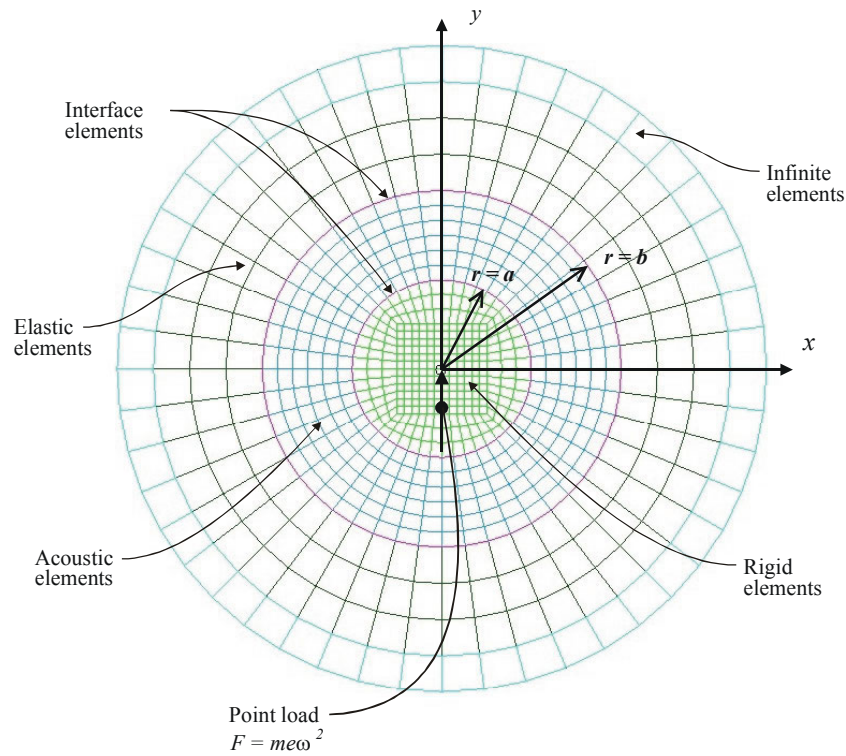
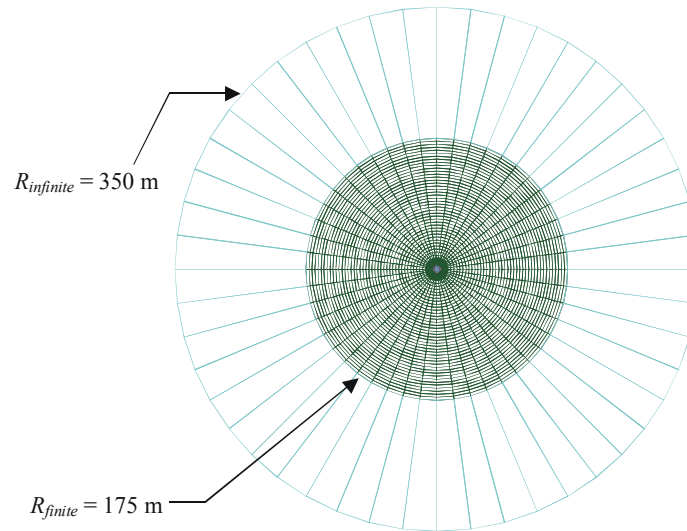


Figure 4. Scaled view of two-dimensional finite element model.

In the finite element model, the boundary conditions of continuity in displacement, continuity in normal stress, and vanishing shear stress between the elastic medium and the acoustic medium were satisfied through the use of the interface element ASI2. The ASI2 element is a two-dimensional, linear, two-node element with displacements in the x - and y -directions and acoustic pressure as the active degrees of freedom. The boundary condition between the orbital vibrator and the acoustic medium in the annulus (5) was modeled by defining the elements of the orbital vibrator as rigid elements and surrounding the rigid elements by ASI2 elements.

The orbital vibrator elements were assigned the elastic properties of steel (Young's modulus $E = 200$ GPa, Poisson's ratio $\nu = 0.29$, mass density $\rho_s = 7820$ kg/m³) and the acoustic elements were assigned the properties of water (mass density $\rho = 1000$ kg/m³, and sound speed $c = 1500$ m/s). A point load F was applied at the center of the orbital vibrator, and the magnitude of the load was calculated using the term $me\omega^2$, which is the force amplitude for a imbalanced rotating-mass. This force was applied in the y -direction. A frequency of 100 Hz was used, or $\omega = 2\pi(100$ Hz). The value of me was taken to be $4.9(10)^{-3}$ (kg-m)/m. Thus, the magnitude of the point load applied to the center of the orbital vibrator was 1934 N. Recall that these numbers were per unit length. Radii of $b = 4.375$ m and $a = 2.1875$ m where chosen for the dimension of the borehole and vibrator respectively. The dimensions, material properties, and force were used correspondingly

in the analytical model. The finite/infinite element boundary was placed at $R_{finite} = 175$ m and therefore the “edge” of the finite model was $R_{infinite} = 350$ m per the instructions for the creation of the infinite element in the ABAQUS user’s manual (2003). Figure 5 provides an overall view, dimensions, and details of the model.



Large Benchmark Model 3216 Elements	
Number of elements per longitudinal - wavelength (15 m) in water	Radius (m)
45	2.1875 – 4.375 (water annulus)
Number of elements per shear - wavelength (31.95 m) in steel	Radius (m)
36	4.375 – 15
8	15 – 175
Number of Circumferential Elements	Number of Circumferential Elements per Wavelength
48	1.3

Figure 5. Mesh properties of the two-dimensional finite element model.

For problems that include an unbounded domain, it is important that the boundary condition at the edge of a finite element model minimize reflected waves. An infinite domain can be modeled numerically by applying what is known as a “quiet” boundary condition at the edge of a finite domain. The quiet boundary condition acts to damp the reflected wave at the finite/infinite

boundary. The quiet boundary condition as defined by the ABAQUS Theory Manual Version 6.3.3 (2003) is

$$\sigma_{xx} = -d_L \dot{u}_x, \quad \sigma_{xy} = -d_S \dot{u}_y, \quad \text{and} \quad \sigma_{xz} = -d_S \dot{u}_z. \quad (10, 11, 12)$$

In the boundary condition equations (10, 11, and 12) σ is the stress, \dot{u} is the velocity and d_L and d_S are the damping constants defined as

$$d_L = \rho c_L \quad \text{and} \quad d_S = \rho c_S. \quad (13, 14)$$

In the impedance equations (13) and (14) ρ is the mass density, c_L is the longitudinal wave speed, and c_S is the shear wave speed of the elastic media. The quiet boundary condition can be applied in ABAQUS by correctly defining infinite elements at the finite/infinite boundary as described in the ABAQUS Standard User's Manual Version 6.3.3 (2003).

The reason that this model is so large is due to a geometry issue with the solid modeling software. According to ABAQUS engineers, the infinite elements must be placed at least $\frac{1}{2}$ a wavelength from the acoustic source. At 100 Hz the longitudinal wavelength in steel is approximately 60 m. This means that if the finite/infinite element boundary were placed at 30 m the "edge" of the model would be placed at 60 m as required for the infinite element to function properly. A nominal radius of an orbital vibrator is 0.05 m. The ratio of outer to inner radii would be $(60/0.05)$ 1200. Difficulties in creating this type of solid-model geometry precluded using the nominal size of the orbital vibrator and placing the finite/infinite element boundary $\frac{1}{2}$ wavelength away. The size of the model was determined by ensuring the value ka was still less than one and the finite/infinite boundary was several wavelengths away. The eccentricity and load applied to the model were arbitrary. Steel properties were used for convenience. In section 3, however, the results from a realistically sized model with elastic properties of an earth material are compared with experimental data.

2.1.1 Two-Dimensional Finite Element and Analytical Model Calculations

The acoustic pressure, and elastic displacement calculations were compared for the finite element and analytical models. The black circles in Figure 6 highlight the locations where the calculations of pressure are reported. These black circles form a line in the direction of oscillation. Figure 7 shows the locations where the displacement calculations are reported, which are also highlighted by black circles in the dark green mesh. One of the lines formed by the black circles is in the direction of oscillation (y -direction) and the other is orthogonal to the direction of oscillation (x -direction). The finite element and analytical model predictions are compared in Figures 8, 9, and 10. These figures show the finite element and analytical predictions for the acoustic pressure (p), elastic displacement in the x - and y -direction (u_x , and u_y) vs. distance from the origin on the y -axis (see Figure 4.), and elastic displacement in the x - and y -direction vs. distance from the origin on the x -axis, respectively.

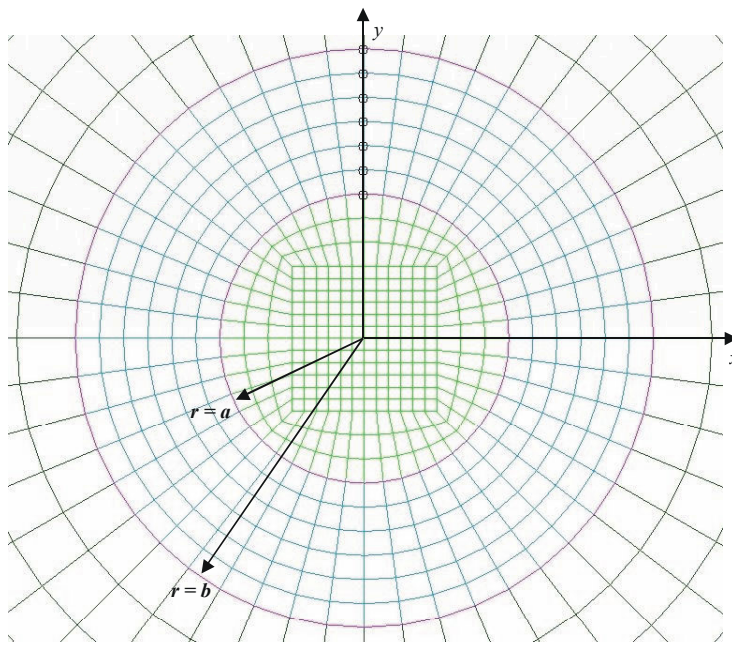


Figure 6. Location of acoustic pressure calculations in the finite element model.

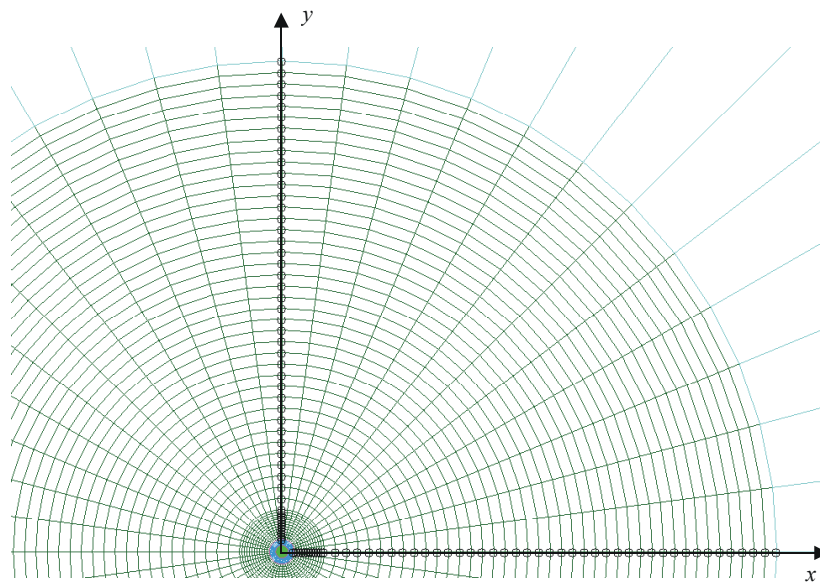


Figure 7. Locations of displacement calculations in the finite element model.

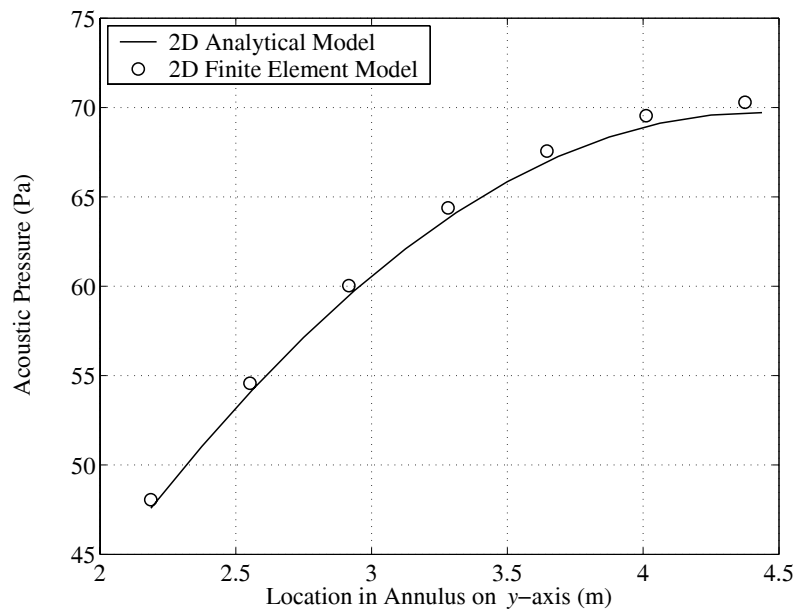


Figure 8. Acoustic pressure in annulus.

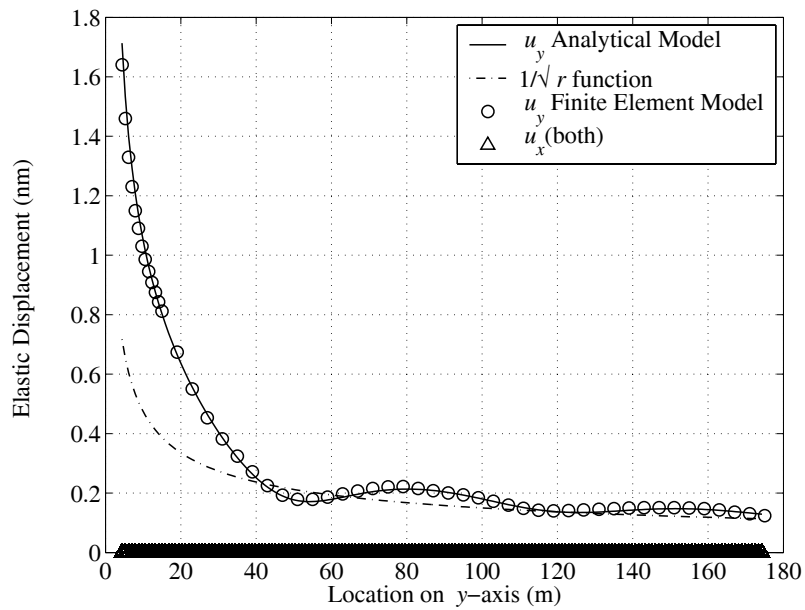


Figure 9. Analytical and finite element displacement calculation on the y-axis.

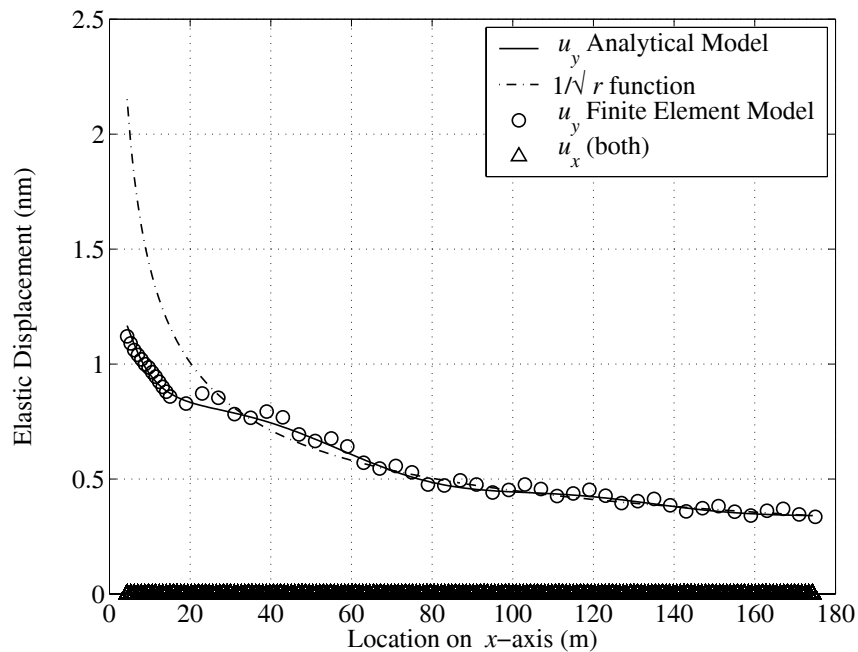


Figure 10. Analytical and finite element displacement calculation on the x-axis.

2.1.2 Summary of models

Figure 8 shows that there is correlation between the analytical and finite element acoustic pressure prediction. Figures 9 and 10 show that the analytical and finite element calculations for u_y on the y-axis and the x-axis are nearly identical. The displacement in the x-direction (u_x) is also zero for both models, which is expected due to the dipole nature of the loading. Also included in Figures 9 and 10 is a $1/\sqrt{r}$ function that is an example of how displacement decreases as the distance from a line source increases in the far-field of an infinite fluid domain (Morse and Ingard, 1968). The comparison between finite element and analytical model calculations shown in Figures 8, 9, and 10 are adequate to conclude that the finite element model was functioning correctly according to theory.

3. Theoretical, ABAQUS, and Experimental Results.

An experiment was conducted in which an orbital vibrator was placed in a liquid-filled steel-cased wellbore. The depth of the orbital vibrator was 2654 feet where the lithology surrounding the well was limestone. Velocity amplitude and frequency of the orbital vibrator were recorded. The radius of the borehole was $b = 0.0762$ m. The radius of the orbital vibrator was $a = 0.04445$ m. The mass per unit length of the orbital vibrator was $M = 9.45$ kg/m. The value of the eccentricity was $me = 4.725(10)^{-4}$ (kg-m)/m.

Analytical and finite element models were created to model this experiment. The liquid in the well was modeled as water with mass density $\rho = 1000 \text{ kg/m}^3$ and pressure wave speed equal to $c = 1500 \text{ m/s}$. The material properties of limestone (Farmer, 1968) were Young's elastic modulus $E = 78.5 \text{ GPa}$, Poisson's ratio $\nu = 0.202$, and mass density $\rho_L = 2500 \text{ kg/m}^3$. The same finite elements were used for this model that were described in section 2 (see Figures 4 and 5 also). R_{finite} and R_{infinite} were 12 m and 24 m respectively. This finite element model is basically the same as the one described in section 2, just smaller. The input for these models was the steady state frequency that was recorded in experiment. The velocity amplitude of the vibrator was then calculated.

Figure 11 shows the orbital vibrator velocity amplitude on the vertical axis and steady-state frequency on the horizontal axis for the theoretical, finite element, and experimental results.

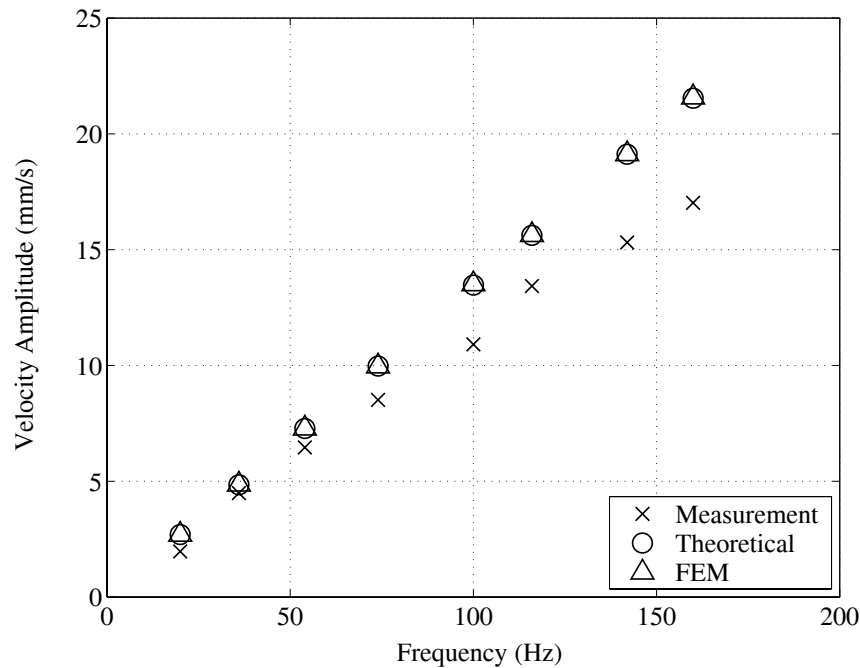


Figure 11. Velocity amplitude calculation and measurement.

Figure 11 shows excellent agreement between theory and finite element calculation for orbital vibrator velocity amplitude. Differences between measurement and calculation were smallest at 36 Hz (7.4%) and largest at 160 Hz (21%). Overall, the difference between measurement and calculation increases with increasing frequency. One reason for the difference between measurement and calculation may be due to the presence of a damping mechanism in the experiment that is absent in the models.

Note that while the velocity calculation for the analytical and finite element solutions are very close, the displacements in the far field were not. This is because the finite/infinite element boundary was approximately $\frac{1}{4}$ of a wavelength from the source, which is about $\frac{1}{2}$ the ABAQUS-recommended distance.

4. Conclusions

A favorable comparison has been made between an ABAQUS finite element model and a theoretical model of an orbital vibrator in a liquid-filled borehole. Calculations for the acoustic pressure within the borehole and the elastic displacements over three wavelengths were nearly identical for the models. Calculations of orbital vibrator velocity amplitude were also nearly identical between the two models and compared favorably to an experimental data set. Based on these results the ABAQUS model is judged to be adequate for calculations of this kind and will be used to investigate which properties of the medium that surrounds a borehole affect the motion of the orbital vibrator especially for cases where analytical solutions are difficult to derive.

5. Acknowledgements

This work was supported by the INEEL LDRD program under DOE contract #DE-AC07-99ID13727.

6. References

1. ABAQUS Theory Manual, Version 6.3.3, 2003, ABAQUS Inc.
2. Brie, A., Endo, T., Hoyle, D., Codazzi, D., Esmersoy, C., Hsu, K., Denoo, S., Mueller, M., Plona, T., Shenoy, R., and Sinha, B., 1998, New directions in sonic logging, Oilfield Review, Schlumberger publication.
3. Chang, C., Coates, R., Dodds, K., Esmersoy, C., and Foreman, J., 1998, Localized maps of the subsurface, Oilfield Review, Schlumberger publication.
4. Daley, T. and Cox, V. D., 2001, Orbital vibrator seismic source for simultaneous P- and S-wave crosswell acquisition, Geophysics, Vol. 66, No. 5, pp. 1471-1480.
5. Farmer, I. W., 1968, Engineering properties of rocks, E. & F. N. Spon LTD.
6. Ihlenburg, F., 1998, Finite element analysis of acoustic scattering, Applied Mathematical Sciences 132, Springer-Verlag New York, Inc., (ISBN 0-387-98319-8).
7. Malvern, L. E., 1969, Introduction to the mechanics of a continuous medium Series in engineering of the physical sciences, Prentice-Hall.

8. Morse, P. M., and Ingard, K. U., 1968, Theoretical acoustics, Princeton University Press, (ISBN 0-691-08425-4).
9. National Research Council – Board on Radioactive Waste Management Water Science and Technology Board, 2000, Research needs in subsurface science, National Academy Press, (ISBN 0-309-06646-8).
10. Paillet, F. L. and Cheng, C. H., 1991, Acoustic waves in boreholes, CRC Press Inc, (ISBN 0-8493-8890-2).
11. Reynolds, R. R. and Cole, J. H., 2002, Propagation from a fluid-encased vibrator in an elastic continuum, XXI Southeastern Conference on Experimental and Applied Mechanics, May 10-21, Orlando, FL.
12. Steidel, R. F., 1989, An introduction to mechanical vibrations, John Wiley & Sons, (ISBN 0-471-84545-0).
13. Williams, E. G., 1999, Fourier acoustics: Sound radiation and nearfield acoustical holography, Academic Press, (ISBN 0-12-753960-3).